

SIMULATION OF FLOW IN SINGLE AND DOUBLE-SIDED LID DRIVEN SQUARE CAVITIES BY DIRECT SIMULATION MONTE CARLO METHOD

by

Deepak NABAPURE and Ram Chandra Murthy KALLURI*

Department of Mechanical Engineering, Birla Institute of Technology and Science,
Pilani, Hyderabad Campus, Hyderabad, India

Original scientific paper

<https://doi.org/10.2298/TSCI180906066N>

The gaseous flow of monoatomic Argon in a double-sided lid-driven square cavity is investigated using the direct simulation Monte Carlo method for different degrees of rarefaction. The effect of the direction of wall motion and the magnitude of wall velocities on the flow physics are analyzed. Unlike the single-sided cavity flow, the double-sided cavity flow generates different vortex formations especially for the parallel wall motion of the wall. The problem, therefore, merits a thorough study, which is attempted in the present paper using the direct simulation Monte Carlo method. Certain complex flow phenomena which are not captured using the numerical methods for continuum flows are revealed by the current method employed in the study. Two counter-rotating vortices are observed for the parallel wall motion whereas only one primary vortex can be observed for the antiparallel case. The variation in the flow and thermal properties is found to be significant at the onset of the transition regime and much smaller in the free molecular regime.

Key words: *discrete methods, direct simulation Monte Carlo, kinetic theory, Knudsen number, lid driven cavity, rarefied gas-flows*

Introduction

For the past several decades, CFD benchmarking of the lid driven cavity flow was and continues to be one of the widely investigated problems [1]. Its technical and scientific importance stems from the ability to depict almost all fluid phenomena such as vortex dynamics, hydrodynamic stability, flow bifurcations and transition to turbulence from an elementary geometrical setting [2]. In this paper, the problem simulated belongs to the category of internally bounded cavity flows in which one or more boundaries are moving and in turn impart motion the fluid. There are many industrial applications of the considered lid-driven cavity flow problem in the fields of coating and drying technologies, melt spinning, aircraft industry to name a few. The cavity problem is also one of the widely studied problems from academic research viewpoint [3].

The flows in the aforementioned cavities can occur in a broad spectrum of rarefaction regimes such as continuum, slip, transition and free molecular. Knudsen number is the quantity which determines the degree of departure from the continuum assumption of fluid. Knudsen number is defined as the ratio of the mean free path, λ , to the characteristic dimension, L , of the system under consideration [4, 5]. Based on the Knudsen number, the flows are classified into

* Corresponding author, e-mail: rcmurthy@hyderabad.bits-pilani.ac.in

four regimes [6]: $0 < \text{Kn} \leq 0.001$ (continuum), $0.001 < \text{Kn} \leq 0.1$ (slip), $0.1 < \text{Kn} \leq 10$ (transition), and $\text{Kn} > 10$ (free molecular). The Knudsen number is also defined in terms of Reynolds number and Mach number by the following relationship.

$$\text{Kn} = \sqrt{\frac{\pi\gamma}{2}} \frac{\text{Ma}}{\text{Re}}, \text{ where } \text{Re} = \frac{\rho U_w L}{\mu} \text{ and } \text{Ma} = \frac{U_w}{\sqrt{\gamma RT}} \quad (1)$$

In the slip flow regime [7] the classical Navier-Stokes equation cannot be used to model the fluid-flow. Velocity slip and temperature jump boundary conditions are applied instead.

Alternate governing equations derived from the Boltzmann equation with a higher order of approximation increases the accuracy of modelling the non-equilibrium flows at the onset of the transition flow regime. However, during the last few years, direct simulation Monte Carlo (DSMC) method articulated by Bird [8] is another popularly used mathematical approach. It solves the Boltzmann equation stochastically and is applied to complex geometries in all the flow regimes ranging from continuum to free molecular flow.

Studies on the single-sided lid-driven cavity have been mostly carried out in the continuum regime, and are often done as a benchmark for validation purposes. During the last few decades, the lid-driven cavity problem has been extensively studied both experimentally and computationally. The single-sided lid-driven cavity flow has been studied extensively by many researchers [9-12] using the conventional numerical methods such as finite element, finite difference, stream function vorticity approach for incompressible flows whereas the DSMC method, the Bhatnagar-Gross-Krook (BGK) method, the unified gas kinetic scheme and the Lattice-Boltzmann method for rarefied flows.

Two-sided cavity problem is another configuration which is essential both from the application and benchmarking viewpoints. In this, the flow is brought about by the tangential movement of two facing cavity boundaries with uniform velocities. The flow is said to have parallel motion if the two walls move in the same direction, and antiparallel if they move in opposite directions. The two-sided cavity problem has been explored computationally and experimentally by many authors [13, 14] in the continuum regime. In a recent study, Bhopalam *et al.* [15] used the Lattice-Boltzmann method to study the two-sided cavity problem having parallel and anti-parallel wall motions. Most of the studies have been performed on incompressible fluid-flows, and very few studies have been performed to analyze the behavior of rarefied flows in the cavities.

In the present study, the DSMC method is used to investigate the rarefied gas-flows for both single-sided cavity flow as well as double-sided cavity flow. Several authors have investigated the thermal and hydrodynamic aspects of rarefied gas-flows in single-sided lid-driven cavities at different degrees of rarefaction using different methods. Microcavity flow in the slip regime was investigated by Auld and Lan [16] using parallel DSMC method. The results obtained from their study agreed well with other computational techniques such as Navier-Stokes equation and Lattice-Boltzmann method. Alkhalidi *et al.* [17] performed a similar study in the slip regime. Mohammadzadeh *et al.* [18] investigated the thermal characteristics of the micro-nanocavity flow in the slip regime using the DSMC method. Their study showed that the conventional approach of using the Navier-Stokes equation along with slip-jump boundary conditions is inaccurate for cavity flows at the border of the slip regime ($\text{Kn} < 0.1$). Furthermore, they introduced the entropy density as one of the tools to determine the non-equilibrium effects and stated the top-left corner of the cavity as the place of maximum entropy density. Mohammadzadeh *et al.* [19] also studied heat flux and entropy behavior in the micro-nanocavities using the DSMC method in the slip and transition regimes. Liu *et al.* [20] investigated the heat transfer in the vacuum package micro-electro-mechanical-systems

devices with constant wall temperature in the continuum and early transition regimes ($Kn = 0.2$). Cai *et al.* [21] performed a similar study in the near continuum and free molecular regimes.

Rana *et al.* [22], applied the finite difference scheme to the lid-driven cavity problem for Knudsen numbers up to 0.7 and compared the steady-state solutions obtained using the regularized 13 moments (R13) equations with the integro moment method and DSMC method. The results obtained were in good agreement among them. Moghadam *et al.* [23] investigated the hydrothermal behavior in cavities using the DSMC method in the slip and transition regime, whereas Eskandari *et al.* [24] studied the same using the time relaxed Monte Carlo scheme. John *et al.* [25] studied the heat transfer phenomena in a lid-driven cavity using the DSMC method in the transition regime. In this study, they showed the existence of heat transfer from cold to a hot region, however, the reason for the same was not stated. In another study, John *et al.* [26] investigated the heat transfer mechanisms in the lid-driven cavity and the effects of incomplete surface accommodation. The study indicated that the surface accommodation greatly influenced flow and heat transfer aspects in the cavity like the vortex center, wall heat flux, and the heat transfer mechanism. Naris and Valougeorgis [27] used the linearized BGK kinetic equation and studied the flow aspects of the lid-driven cavity in all the rarefaction regimes using the DSMC method. In a similar study by Aoki *et al.* [28] used the BGK model to numerically investigate the rarefied flow and the behavior of the molecular velocity distribution function in a square container.

Huang *et al.* [29] formulated a unified gas-kinetic scheme based on the kinetic model and applied the same for the lid-driven cavity flow. They compared the Navier-Stokes solver and the DSMC method and demonstrated that the current kinetic model had superior capability than the conventional Navier Stokes solver in capturing the rarefied flow behavior. Venugopal and Girimaji [30] also used the unified gas-kinetic scheme to study the lid-cavity flow in the near-continuum/slip regime to the rarefied regime and validated the same using the DSMC method. Wu *et al.* [31] investigated the effect of the aspect ratio and the oscillating frequency on the rarefied flow in a lid-driven cavity using the linearized Boltzmann equation. In a recent study, Wang *et al.* [32] investigated the flow and thermal characteristics of oscillatory rarefied flow in a single-sided square cavity using the gas kinetic theory in all the flow regimes. Their study showed that the heat transfer in the cavity was greatly influenced by the oscillating frequency and the velocity of the lid.

Despite the wide-ranging studies focused on lid-driven cavities, all of them were performed for the single-sided cavity, and very few studies have focused on the double-sided cavity. In the present study, we apply the DSMC method to explore the behavior of monatomic gas-flows in a single-sided as well as a double-sided lid-driven cavity in all the rarefaction regimes. According to our literature review, there are no prior studies on rarefied gas flow behavior in double-sided lid-driven cavities using the DSMC method. The present problem hence merits careful study and is taken up in this paper using the DSMC method. The effect of different wall velocities and rarefaction regimes has been studied for both parallel and antiparallel motion of the walls.

The DSMC method

The DSMC developed by Bird [8] is one of the most significant numerical technique to solve problems involving rarefied gas-flows. It is based on the Boltzmann's equation [33] with certain restrictions:

$$\frac{\partial(nf)}{\partial t} + c \frac{\partial(nf)}{\partial r} + F \frac{\partial(nf)}{\partial c} = \int_{-\infty}^{+\infty} \int_0^{4\pi} n^2 (f^* f_1^* - ff_1) c_r \sigma d\Omega dc_1 \quad (2)$$

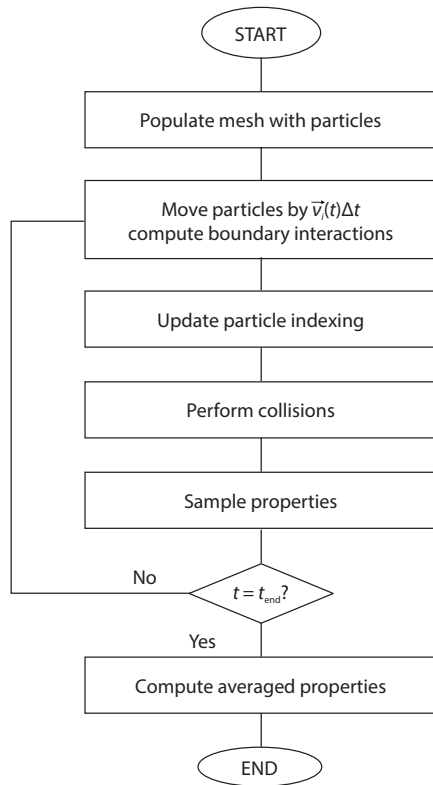


Figure 1. Standard DSMC algorithm flowchart

Equation (2) is an integrodifferential equation in nf , the product of the number density, n , and the velocity distribution function, f . In this equation, c is the molecular velocity, c_r – the relative molecular speed, F – the external force, $*$ – the superscript indicates post-collision values, f and f_i are distribution functions for two different types of molecules, σ – the collision cross-section, and Ω – the solid angle. The right side of the equation is the collision integral, which is the source of problems in finding a solution.

The DSMC method can reasonably predict the flow and heat transfer aspects in all the flow regimes precisely, thus making it one of the most widely used approaches for large-scale rarefied gas simulations [34]. However, it entails specific constraints on the cell size, time step, particles per cell to ensure accuracy, and makes the DSMC method computationally expensive. Statistical noise is another critical factor which influences the accuracy of the solution, and it needs to be minimized. The DSMC method can be easily parallelized, and accurate solutions can be obtained by adopting parallelization techniques which are carried out in the present study. The DSMC algorithm has four main phases: the motion of the particles, re-indexing the particles, calculating the collisions, and sampling the flow field. The basic DSMC algorithm flowchart is shown in fig. 1.

Geometry definition

In the present paper, the lid-driven cavity simulated for different cases, is as shown in the fig. 2. According to fig. 2, L is the edge length of the square cavity. The corners of the cavity are labeled A, B, C, and D in that order. In the first case, it was considered that the top wall moves with a fixed tangential velocity of U_w in the positive x -direction, with the other walls being stationary and in the second case both walls move either in parallel or antiparallel directions with a fixed tangential velocity of U_w .

The variation in the Knudsen number is achieved by changing the density which is dependent on the reference pressure under which the simulation is carried out. The mean free path is given:

$$\lambda = \frac{\mu}{P_0} \sqrt{\frac{\pi R T_0}{2}}$$

where μ is the the viscosity of the gas which depends on the initial temperature T_0 . The boundary conditions for both parallel motion and antiparallel motion are shown in the fig. 2.

Computational methodology

All the simulations in the present study were performed with an opensource C++ parallel DSMC code known as *dsmcFoam* under the framework of OpenFOAM. For all the flow calculations, monoatomic gas, Argon, was considered. The variable hard sphere (VHS)

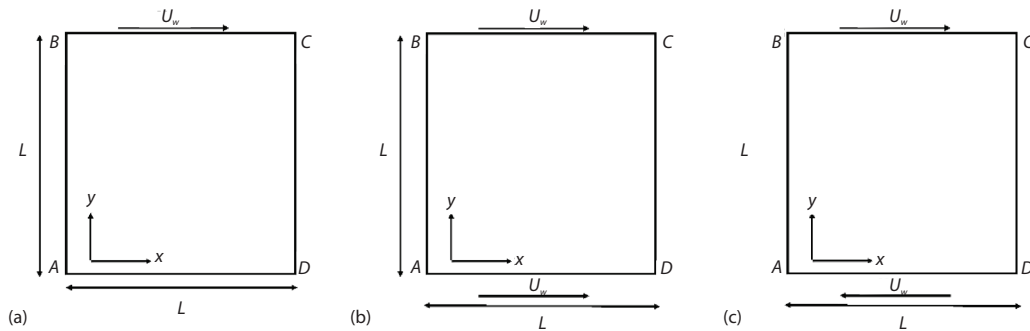


Figure 2. Flow configuration of the single and double-sided cavity flow problems; (a) single-sided flow with moving top wall, (b) double-sided flow with parallel wall motion, and (c) double-side flow with antiparallel wall motion

molecular model and the no time counter collision sampling technique is used to model the collision kinetics. The wall interactions are assumed to be inelastic with diffuse reflection model and having full thermal accommodation. The bulk flow is neglected in the z -direction making it a 2-D problem. The problem is simulated for different wall velocities U_w such as 10, 50, 100, and 200 m/s. The simulation parameters are listed in tab. 1, and the different cases considered are listed in tab. 2.

Table 1. Simulation parameters

Quantity	Parameters	Quantity	Parameters
Length [m]	1 m	Gas-wall interaction	Diffuse reflection
Height [m]	1 m	Gas-gas interaction	VHS
Reynolds number	0.05-1.05	Initial gas temperature, T_0	273 K
Mach number	0.032-0.64	Wall temperature, T_w	273 K
Viscosity, μ	$2.1 \cdot 10^{-5}$ Ns/m ²	Working fluid	Argon
Viscosity temperature index, ω	0.81	Molecular mass, m	$6.63 \cdot 10^{-26}$ kg
Aspect ratio	1	Molecular diameter, d	$4.17 \cdot 10^{-10}$ m

Table 2. List of cases studied

n_∞ [1m ⁻³]	U_w [ms ⁻¹]	p_∞ [Nm ⁻²]	ρ_∞ [kgm ⁻³]	Kn	Regime
$1.6658 \cdot 10^{21}$	50	6.27	$1.10 \cdot 10^{-4}$	0.001	Continuum
$1.6658 \cdot 10^{20}$	50	0.627	$1.10 \cdot 10^{-5}$	0.01	Slip
$3.3316 \cdot 10^{19}$	50	0.125	$2.20 \cdot 10^{-6}$	0.05	Slip
$1.6658 \cdot 10^{19}$	50	0.0627	$1.10 \cdot 10^{-6}$	0.1	Slip
$3.3316 \cdot 10^{18}$	50	0.0125	$2.20 \cdot 10^{-7}$	0.5	Transition
$1.6658 \cdot 10^{18}$	50	$6.27 \cdot 10^{-3}$	$1.10 \cdot 10^{-7}$	1	Transition
$3.3316 \cdot 10^{17}$	50	$1.25 \cdot 10^{-3}$	$2.20 \cdot 10^{-7}$	5	Transition
$1.6658 \cdot 10^{17}$	50	$6.27 \cdot 10^{-4}$	$1.10 \cdot 10^{-8}$	10	Transition
$1.11 \cdot 10^{17}$	50	$4.18 \cdot 10^{-4}$	$7.35 \cdot 10^{-9}$	15	Free molecular
$8.32 \cdot 10^{16}$	50	$3.13 \cdot 10^{-4}$	$5.51 \cdot 10^{-9}$	20	Free molecular

Grid independence, timestep independence, and validation of single lid-driven square cavity

The *dsmcFoam* solver is used to compute the flow inside a single lid-driven square cavity, where the top lid moves from left to right. The flow domain is equally divided in x - and y -directions. Grid independence test was carried out for four different mesh sizes – coarse, medium, fine, finer, *i. e.*, 50×50 , 75×75 , 100×100 , and 125×125 as shown in fig. 3(a). The variation in results for the medium and fine grid was not significant. Hence a structured grid of 100×100 was used for the rest of the study.

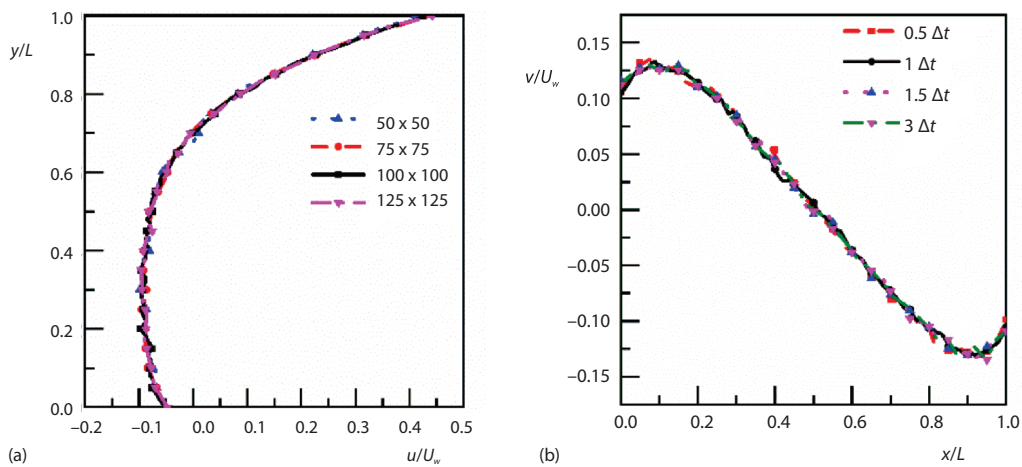


Figure 3. Grid and time-step independence results; (a) u velocity profile along a vertical line, (b) v velocity profile along a horizontal line

Similarly, independence test was carried out for four different timesteps, *i. e.*, $0.5\Delta t$, $1\Delta t$, $1.5\Delta t$, and $3\Delta t$ as shown in fig. 3(b). The variation in results is negligible, and hence a timestep $\Delta t = 2 \cdot 10^{-6}$ s was considered in the present study, and it was also much smaller than

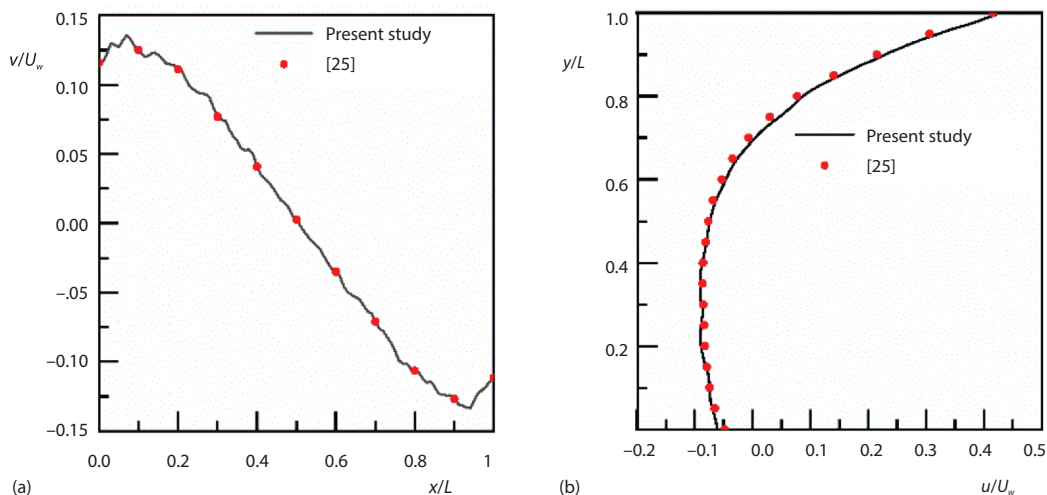


Figure 4. (a) Computed v velocity profile along a horizontal line, (b) u velocity profile along a horizontal line, compared with [25]

the mean collision time. The DSMC particles initialized per cell were 25, and it resulted in a total number of simulated particles of around five lakhs. All the simulations were carried out on a 16 Core Processor. Each of the simulations took about 26-28 hours.

Numerical results for a single lid-driven cavity flow for $Kn = 1$ and $U_w = 50$ m/s by John *et al.* [25] exist for this problem. The agreement between the DSMC results from the present study and those of John *et al.* [25], as shown in figs. 4(a) and 4(b) is excellent, validating the *dsmcFoam* solver.

Comparison of DSMC results with NSF and R13 for double-sided lid-driven cavity with antiparallel wall motion

The flow features in the slip regime were also simulated using the Navier-Stokes Fourier (NSF) approach, DSMC based modelling and the same have been compared with the R13 solutions from the literature [35]. Double-sided lid-driven cavity flow with antiparallel wall motion has been simulated for $Kn = 0.01$ and $U_w = 50$ m/s. The COMSOL multiphysics with velocity slip conditions has been used to solve the Navier-Stokes equation. Figure 5 shows the comparison of the u -velocity component normalized by most probable speed along the vertical centerline. Figure 6 shows the velocity streamlines obtained using the DSMC method and the NSF method. From these figures, we see a good agreement between the three approaches. The velocity streamlines shown here for low Knudsen number, have dumbbell shaped vortices at the center, inclined towards the direction of driving walls. As seen in fig. 12 in section *Double-sided lid-driven cavity flow with anti-parallel wall motion*, the streamlines merge into a single large symmetric vortex at the center, for higher Knudsen number.

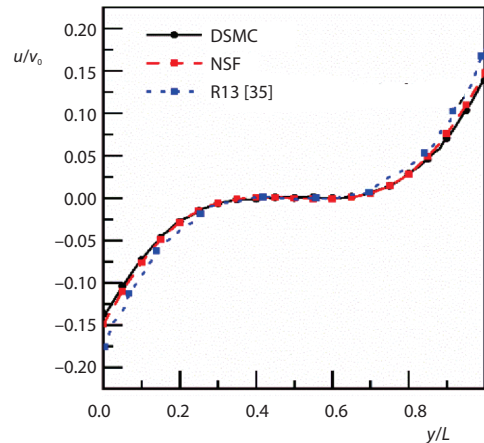


Figure 5. Velocity profiles predicted by the DSMC, NSF and R13 methods

Results and discussion

Selected results ($Kn = 0.01, 0.1, 1, 10,$ and 20) obtained using DSMC method are shown for two configurations: double-sided lid-driven cavity flow with: parallel and anti-parallel wall motions. Two different sets of simulations were performed for each of these configurations: to assess the impact of flow in the cavity, lid velocities of $U_w = 10, 50, 100, 200$ m/s were considered with $Kn = 1$ and subsequently, to study the rarefaction effect on the flow, Knudsen number was varied, and U_w was fixed at 50 m/s.

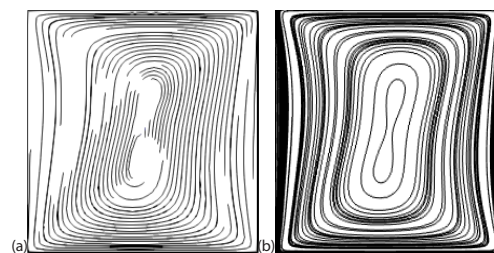


Figure 6. Comparison of the velocity streamlines for antiparallel wall motion using: (a) DSMC, (b) NSF method for $Kn = 0.01, U_w = 50$ m/s

Double-sided lid-driven cavity flow with parallel wall motion

Effect of lid velocities

Figure 7 shows the velocity streamlines superimposed on the pressure contours for different wall velocities for parallel wall motion. The profiles for $U_w = 50, 100$ m/s are similar and hence not shown.

It is observed that the top left corner of the cavity has a significant drop in pressure whereas the top right corner has a significant pressure rise. This can be attributed to the expansion of the fluid at the top left corner, and compression in the other corner due to the lid motion. For the case 7(a) where the lid velocity is 10 m/s, the pressure is relatively constant throughout the domain. The pressure changes are more for higher lid velocities. From the velocity streamlines two symmetric and counter-rotating primary vortices are visible. The vortex centers shift towards the right side of the flow domain for higher lid velocities.

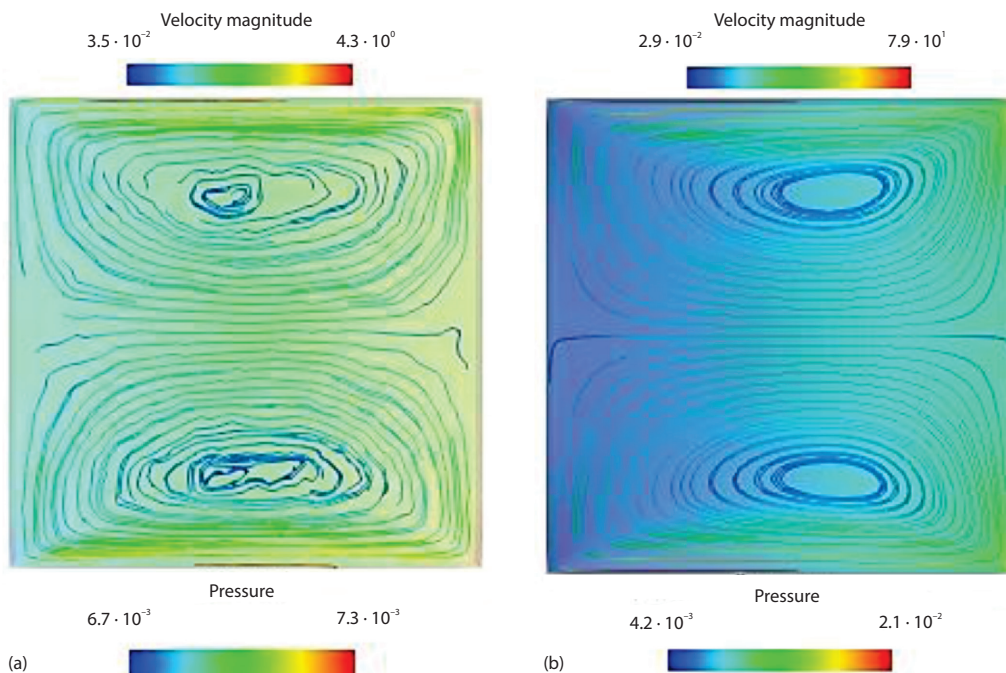


Figure 7. Velocity streamlines overlaid on pressure, Pa, contours for (a) $U_w = 10$ m/s, (b) $U_w = 200$ m/s

Temperature contours in the flow domain are shown in fig. 8. The maximum temperature in the flow can be seen to increase with increasing lid velocities. It is also observed that cold region exists on the left side wall for all the lid velocities. The hot region is observed on the right side edge for low lid velocities. In contrast to the cold region, the hot region shifts from the right side edge and moves towards the driving walls for increasing lid velocities. This can be attributed to the compression effects for low velocities and viscous dissipation at higher velocities as it is primarily observed near the driving walls. The normalized heat flux profiles along the walls for different wall velocities are shown in fig. 9. They follow a similar trend as temperature with peaks at corners 2 and 3.

Effect of rarefaction

Velocity profiles. From the u -velocity profile in figs. 10(a) and 10(b) it can be observed that the profiles are symmetric about the horizontal centerline, and the velocity decreases first and then increases. It is interesting to note that the drop in velocity is more for $Kn = 0.01$. For higher Knudsen number, there exists a large slip between the driving walls and the adjacent fluid layers as expected. Thus, lesser kinetic energy is imparted to the flow resulting in smaller velocities of the fluid layers along the driving walls. This also manifests as smaller flow velocities along the horizontal centerline

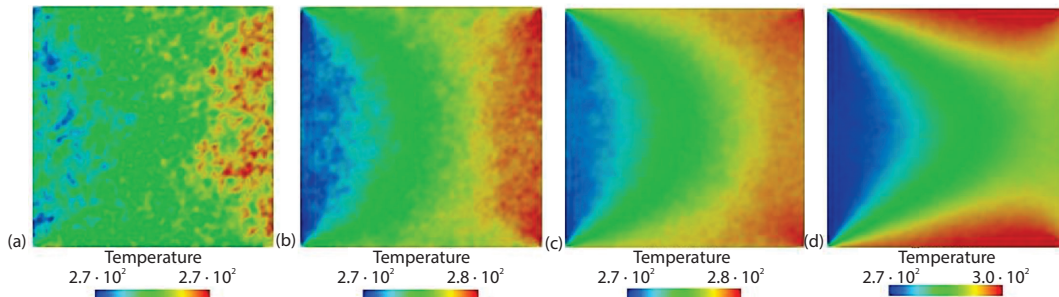


Figure 8. Temperature [K] contours for (a) $U_w=10$ m/s, (b) $U_w= 50$ m/s, (c) $U_w= 100$ m/s, and (d) $U_w= 200$ m/s

as seen from fig. 10(a). A similar trend is observed along the vertical centerline as seen from fig. 10(b). The v -velocity component fluctuated about its mean value of zero only by 1% and hence the same is not depicted.

Temperature profiles. Figures 10(c) and 10(d) show the temperature profile variation along the horizontal and vertical centerline, respectively for different rarefaction regimes. The plots show an large variation of temperature near the side walls as the flow progresses from the slip to the transition regime. In the slip regime, the temperature deviation from the initial value is negligible. The increase in Knudsen number leads to further deviation in the gas temperature away from the initial temperature of the flow field, due to increasing non-equilibrium effects, particularly near the left and right sides of the cavity. The increase/decrease in the flow temperature at the right and left sides of the cavity is slightly more for the free molecular regime. From fig. 10(e), we see that the deviation in non-dimensional temperature is high in magnitude near the driving walls compared to that along the centerlines of the domain due to high viscous dissipation.

Pressure profiles. Comparison of pressure along a horizontal and vertical line crossing the center of the cavity are shown in fig 10(f) and 10(g). The trend of pressure variation is similar to that of temperature profile. It can be observed that the pressure variation along the horizontal centerline remains relatively uniform in the slip regime, whereas there is a significant pressure change in other regimes. The curves overlap for higher Knudsen number cases indicating that the number density has minimal effect on the pressure fluctuations in the transition and free molecular regimes. Along the vertical centerline, the pressure change is however negligible. A common feature among the velocity, temperature and pressure plots is that the change in profiles is more pronounced at the onset of the transition regime (particularly about $Kn = 0.1$) as compared to the slip or free molecular regimes.

Heat flux profile. The variation in heat flux along the four walls of the cavity, as a function of Knudsen number, are shown in fig. 11. In this figure, $q_0 = \mu RT_0/L$ is used to non-dimensionalise the heat-flux profiles. The variation in heat flux along the walls is more prominent in the slip regime. With increase in Knudsen number, the variations in heat flux along the walls

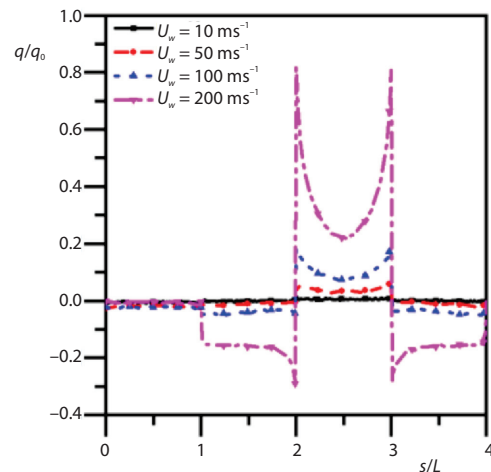


Figure 9. Comparison of the heat flux profiles along the walls of the cavity

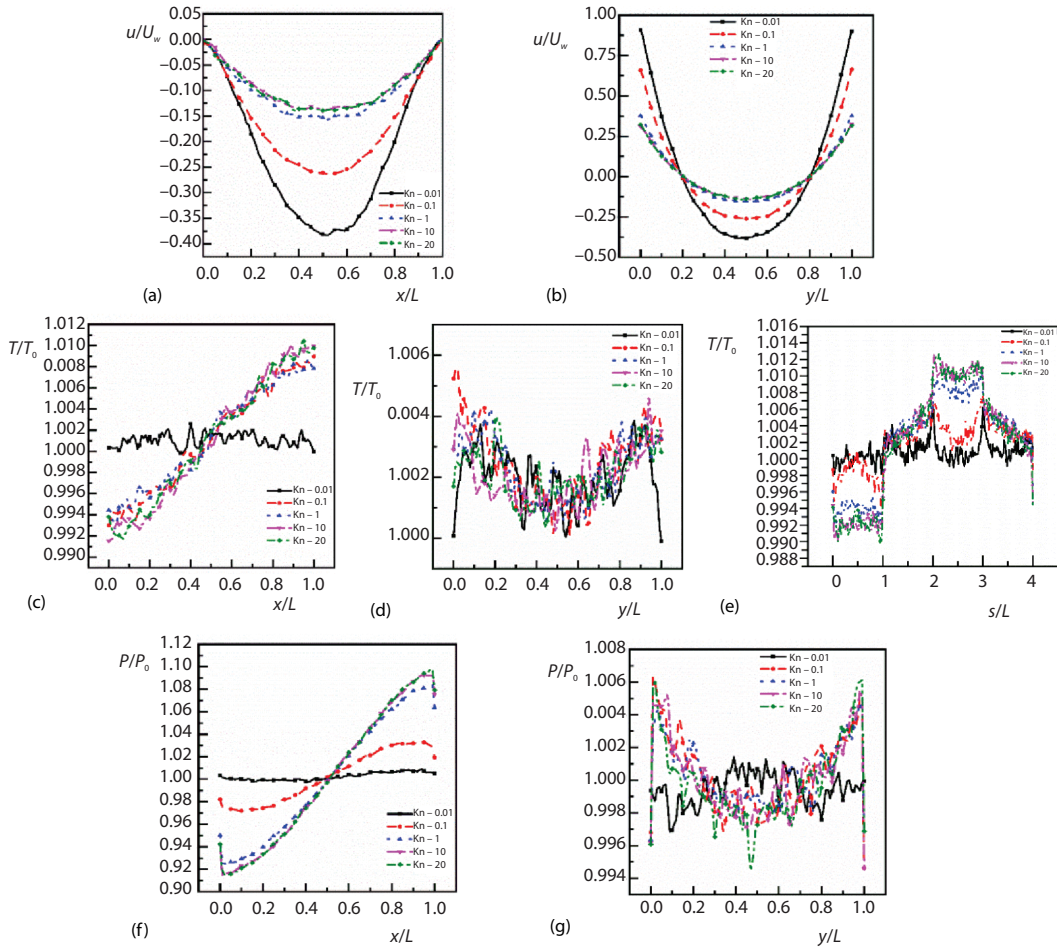


Figure 10. Comparison of non-dimensional velocity (a, b), temperature (c, d) and pressure (f, g) profiles along the horizontal and vertical centerlines, and (e) temperature along the walls of the cavity for different Knudsen number

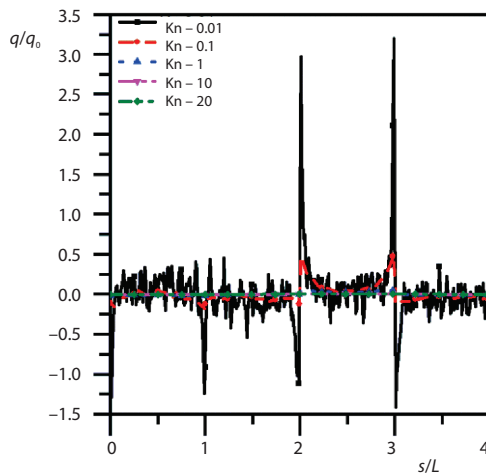


Figure 11. Comparison of the heat flux profiles along the walls of the cavity

reduce and tend to zero. Energy gain or loss of the molecules occur when they interact with the cavity walls. Heat is absorbed from the surroundings by the cavity in the top left corner due to expansion. At higher Knudsen number, compression and viscous dissipation effects due to the driving walls lead to a higher gas temperature near the right-side wall. This results in the heat flux peaks as observed at the corners 2 and 3.

Double-sided lid-driven cavity flow with anti-parallel wall motion

Effect of lid velocities

Figure 12. shows the velocity streamlines superimposed on pressure contours for different wall velocities with antiparallel wall motion. As seen from fig. 12, the maximum flow velocity in the domain, which occurs adjacent to the driving walls, is almost half that of the driving wall velocity. This shows that there is a definite slip between the driving wall and the fluid layer adjacent to it. This is the slip velocity phenomenon typically encountered in the rarefied gas-flows.

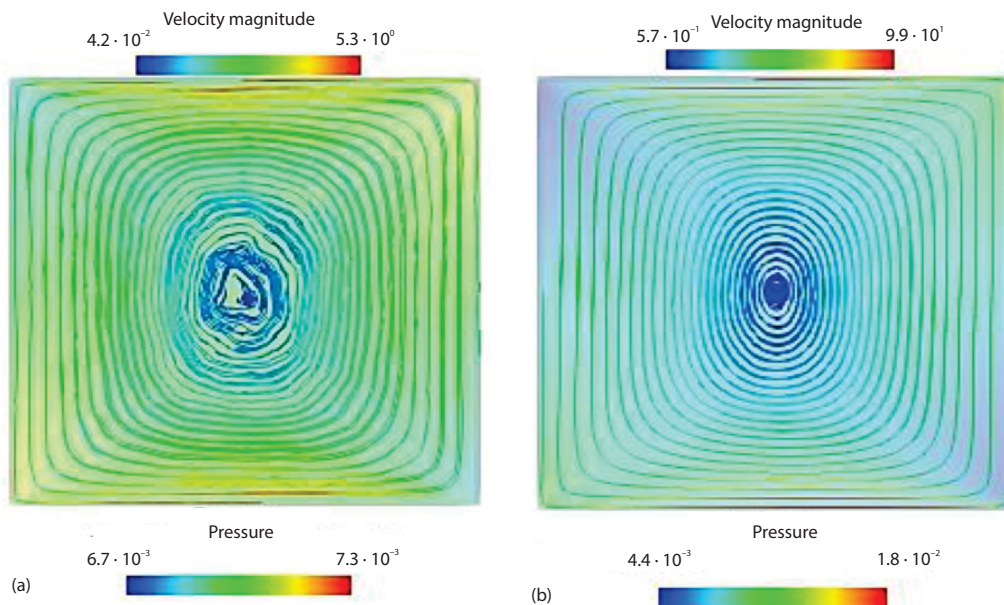


Figure 12. Velocity streamlines overlaid on pressure [Nm⁻²] contours for double sided driven cavity flow for antiparallel wall motion: (a) $U_w = 10$ m/s, (b) $U_w = 200$ m/s

From fig. 12, it can also be seen that the pressure contours are similar to the parallel wall motion case with a low pressure region at the top left corner and a high pressure region at the top right corner with the pressure remaining constant in the center of the domain. Velocity streamlines show that a single primary vortex is formed at the center of the cavity. Increase in the lid velocity has little effect on the center of the primary vortex, and it remains at the center of the cavity unlike the case of parallel wall motion.

The temperature contours, shown in fig. 13, share a common feature with the case of parallel wall motion. For low wall velocities, the regions of high temperature occur at the corners where the high pressure regions exist. With increasing wall velocities, they gradually move closer to the moving walls. It can be attributed to competing factors like compressibility effects and viscous heat generation. Also, the minimum temperature observed in the domain for all the cases is less than a Kelvin below the reference temperature. This difference is due to the rarefac-

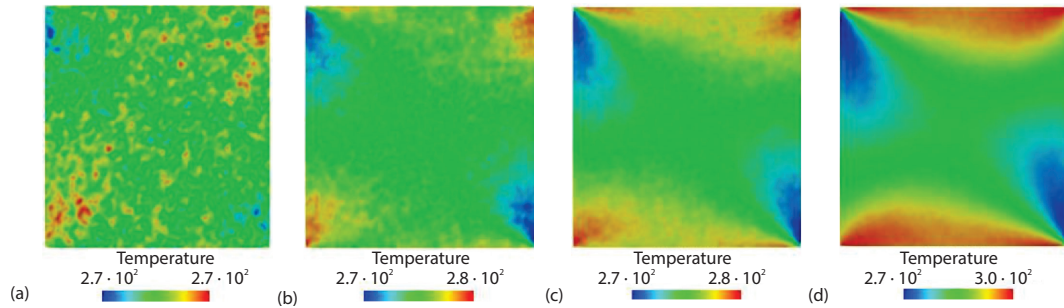


Figure 13. Temperature [K] contours for (a) $U_w = 10$ m/s, (b) $U_w = 50$ m/s, (c) $U_w = 100$ m/s, (d) $U_w = 200$ m/s

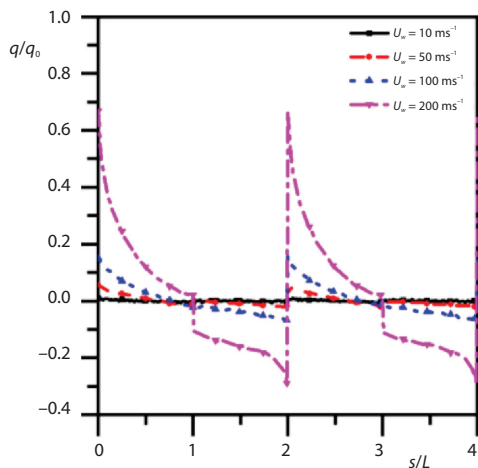


Figure 14. Comparison of the heat flux profiles along the walls of the cavity

Knudsen number, whereas, in the slip regime, considerable variation is observed. Furthermore, the velocity profiles follow a wavy pattern along the length of the cavity. From fig. 15(b) it can be observed that the v -velocity is close to zero for lower Knudsen number at the two extremities of the cavity. As the Knudsen number increases v -velocity slip increases and reaches a finite value. Also, the flow is symmetric about the horizontal centerline. From fig. 15(c) the u -velocity component fluctuates from a minimum to maximum changing direction at the center (*i. e.*, $y/L = 0.5$).

Temperature profiles. Figures 15(e) and 15(f) show the temperature variation along the vertical and horizontal centerline, respectively, for different rarefaction regimes. The plots reveal that the variation of temperature is similar in both the cases as the flow progresses from slip to transition regime with no definitive trend in their variation. From fig. 15(g), we see that the non-dimensional temperatures vary over a broader range when compared with those near the domain centerlines. The peaks in the temperatures are also seen at the corners of the domain as a result of both compression and viscous dissipation effects.

Pressure profiles. Comparison of pressure along vertical and horizontal lines crossing the center of the cavity are shown in fig 15(h) and 15(i). The changes in pressure are more pronounced for higher Knudsen number compared to lower Knudsen number. The pressure is high

tion effects as also seen from the published literature [25]. However, the maximum temperature in the domain, observed near the driving walls is well above the reference temperature of the fluid. This is attributed to the viscous dissipation effects as previously stated.

Normalized heat flux along the walls are shown in fig. 14 for different wall velocities. With increase in the wall velocity, the magnitude of heat flux increases. At lower wall velocity, the heat flux is almost constant. The peaks of heat flux occur at the intersection of two driving walls with the stationary walls.

Effect of rarefaction

The variations in u and v -velocity profiles shown in fig. 15(a)-15(d) are lower for high

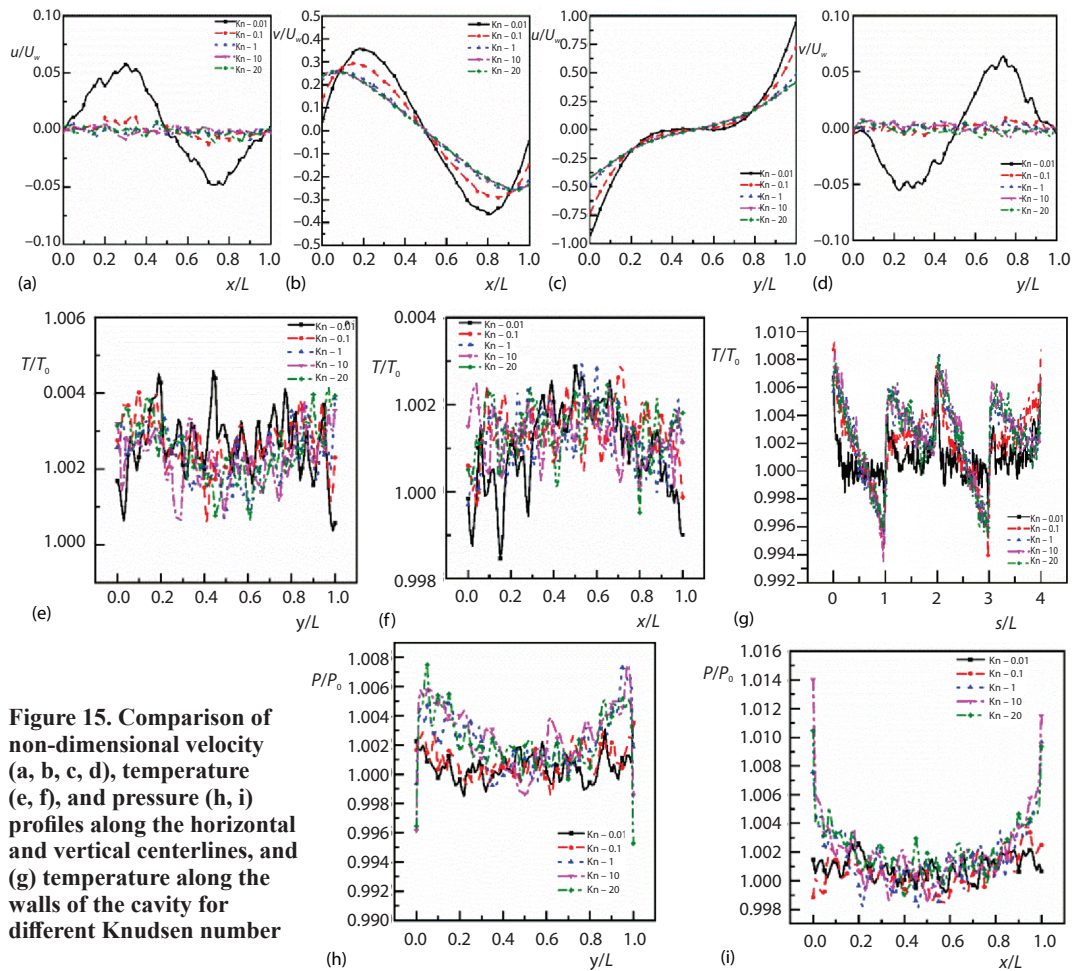


Figure 15. Comparison of non-dimensional velocity (a, b, c, d), temperature (e, f), and pressure (h, i) profiles along the horizontal and vertical centerlines, and (g) temperature along the walls of the cavity for different Knudsen number

at the edges of the cavity, with a pressure drop towards the midpoint of the cavity. In the slip regime, the pressure remains almost constant along the centerlines of the cavity with minor fluctuations about the mean.

As in the case of parallel wall motion, the changes in velocity, temperature and pressure profiles are more pronounced near the beginning of the transition regime (around $Kn = 0.1$).

Heat flux profiles. The variations in heat flux along the four walls of the cavity, as a function of Knudsen number, are shown in fig. 16. In this figure, $q_0 = \mu RT_0/L$ is used to non-dimensionalize the heat-flux profiles. The heat flux is symmetric about the vertical centerline.

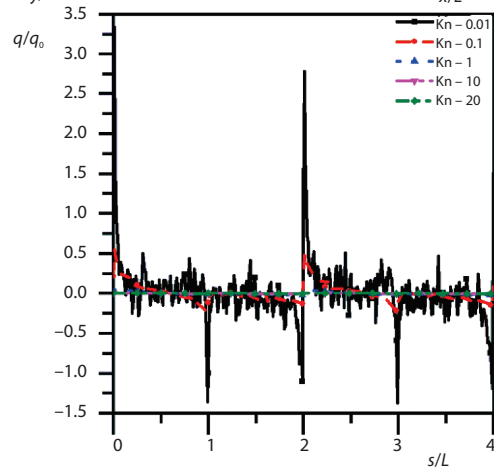


Figure 16. Comparison of the heat flux profiles along the walls of the cavity

The heat flux almost remains constant in the transition and free molecular regimes, whereas higher fluctuations are observed in the slip regime. Figure 16 also illustrates that the maximum heat flux peaks are observed at the intersection of the driving lid with vertical walls *i. e.*, corners 0 and 2 which is due to the accumulation of heat as the flow occurs.

Conclusion

In this work, a relatively unexplored flow configuration in a double-sided lid-driven square cavity is investigated using the DSMC method. The flow is investigated for both parallel and antiparallel motion of the two driving walls. The *dsmcFoam* solver is validated by comparison with the well-established results from the literature. The flow features have been studied for different wall velocities and rarefaction regimes. Two counter-rotating vortices are observed for the parallel wall motion whereas only one primary vortex is observed for the antiparallel case. Physics governing the nature of temperature distribution and heat flux variations in the flow domain is attributed to competing factors like expansion cooling and viscous dissipation. The variation in the flow and thermal properties is significant at the onset of the transition regime and much smaller in the free molecular regime.

Nomenclature

c – molecular velocity, [ms^{-1}]
 d – particle diameter, [m]
 F – external force, [N]
 f – velocity distribution function
 Kn – Knudsen number
 L – characteristic length, [m]
 m – molecular mass, [kg]
 n – number density, [m^{-3}]
 P_0 – reference pressure, [Nm^{-2}]
 p_∞ – pressure, [Nm^{-2}]
 R – gas constant, [$\text{Jmol}^{-1}\text{K}^{-1}$]

r – relative molecular speed, [ms^{-1}]
 T_∞ – temperature, [K]

Greek symbols

λ_∞ – mean free path, [m]
 μ_∞ – viscosity, [Nsm^{-2}]
 ρ_∞ – density, [kgm^{-3}]
 σ – collision cross-section, [m^2]
 Ω – solid angle, [sr]
 ω – viscosity index

References

- [1] Gelfgat, A. Y., Linear Instability of the Lid-Driven Flow in a Cubic Cavity, *Theoretical and Computational Fluid Dynamics*, 33 (2019), 1, pp. 59-82
- [2] Wahba, E. M., Multiplicity of States for Two-Sided and Four-Sided Lid Driven Cavity Flows, *Computers and Fluids*, 38 (2009), 2, pp. 247-253
- [3] Ghia, U., High-Re Solutions for Incompressible Flow Using the Navier-Stokes Equations and a Multigrid Method, *Journal of Computational Physics*, 48 (1982), 3, pp. 387-411
- [4] Barbaros, C., Ozgur, B., Evaluation of Nusselt Number for a Flow in a Microtube Using Second-Order Slip Model, *Thermal Science*, 15 (2011), Suppl. 1, pp. S103-S109
- [5] Rahbar, N., et al., Numerical Investigation on Flow Behavior and Energy Separation in a Micro-Scale Vortex Tube, *Thermal Science*, 19 (2015), 2, pp. 619-630
- [6] Miguel, A., Non-Darcy Porous Media Flow in No-Slip and Slip Regimes, *Thermal Science*, 16 (2012), 1, pp. 167-176
- [7] Milicev, S., Stevanovic, N., Navier-Stokes-Fourier Analytic Solutions for Non-Isothermal Couette Slip Gas-Flow, *Thermal Science*, 20 (2016), 6, pp. 1825-1833
- [8] Bird, G. A., *Molecular Gas Dynamics and the Direct Simulation of Gas-Flows*, Oxford, Oxford University Press, New York, USA, 1994
- [9] Cheng, M., Hung, K. C., Vortex Structure of Steady Flow in a Rectangular Cavity, *Computers and Fluids*, 35 (2006), 10, pp. 1046-1062
- [10] Hamimid, S., et al., Numerical Study of Natural-Convection in a Square Cavity under Non-Boussinesq Conditions, *Thermal Science*, 20 (2016), 5, pp. 1509-1517
- [11] Bennacer, R., et al., Differentiated Heated Lid Driven Cavity Interacting with Tube: A Lattice-Boltzmann Study – Part A: *Thermal Science*, 21 (2017), 1, pp. 89-104

- [12] Su, C.-C., et al., Large-Scale Simulations on Multiple Graphics Processing Units (GPU) for the Direct Simulation Monte Carlo Method, *Journal of Computational Physics*, 231 (2012), 23, pp. 7932-7958
- [13] Kuhlmann, H. C., et al., Flow in Two-Sided Lid-Driven Cavities: Non-Uniqueness, Instabilities, and Cellular Structures, *Journal of Fluid Mechanics*, 336 (1997), Apr., pp. 267-299
- [14] Perumal, D. A., Dass, A. K., Multiplicity of Steady Solutions in 2-D Lid-Driven Cavity Flows by Lattice Boltzmann Method, *Computers and Mathematics with Applications*, 61 (2011), 12, pp. 3711-3721
- [15] Bhopalam, S. R., et al., Computation of Fluid-Flow in Double Sided Cross-Shaped Lid-Driven Cavities Using Lattice-Boltzmann Method, *European Journal of Mechanics – B/Fluids*, 70, (2018), July, pp. 46-72
- [16] Auld, D., Lan, Y., Simulation of Lid-Driven Cavity Flow by Parallel DSMC Method, *Proceedings*, 24th AIAA Applied Aerodynamics Conference, San Francisco, Cal., USA, 2006
- [17] Alkhalidi, A., et al., Rarefaction and Scale Effects on Heat Transfer Characteristics for Enclosed Rectangular Cavities Heated from Below, *Thermal Science*, 23 (2017), 3, pp. 1791-1800
- [18] Mohammadzadeh, A., et al., Thermal and Second-Law Analysis of a Micro-or Nanocavity Using Direct-Simulation Monte Carlo, *Physical Review E*, 85 (2012), 5, 056310
- [19] Mohammadzadeh, A., et al., A Parallel DSMC Investigation of Monatomic/Diatomic Gas-flows in a Micro/NanoCavity, *Numerical Heat Transfer – Part A: Applications*, 63 (2013), 4, pp. 305-325
- [20] Liu, H., et al., Monte Carlo Simulations of Gas-Flow and Heat Transfer in Vacuum Packaged MEMS devices, *Applied Thermal Engineering*, 27 (2007), 2, pp. 323-329
- [21] Cai, C., Heat Transfer in Vacuum Packaged Microelectromechanical System Devices, *Physics of Fluids*, 20 (2008), 1, 017103
- [22] Rana, A., et al., A Robust Numerical Method for the R13 Equations of Rarefied Gas Dynamics: Application Lid Driven Cavity, *Journal of Computational Physics*, 236 (2013), Mar., pp. 169-186
- [23] Moghadam, E. Y., et al., Heat Transfer and Fluid Characteristics of Rarefied Flow in Thermal Cavities, *Vacuum*, 109 (2014), Nov., pp. 333-340
- [24] Eskandari, M., Nourazar, S. S., On the Time Relaxed Monte Carlo Computations for the Lid-Driven Micro Cavity Flow, *Journal of Computational Physics*, 343 (2017), Aug., pp. 355-367
- [25] John, B., et al., Investigation of Heat and Mass Transfer in a Lid-Driven Cavity Under Non-Equilibrium Flow Conditions, *Numerical Heat Transfer – Part B: Fundamentals*, 58 (2010), 5, pp. 287-303
- [26] John, B., et al., Effects of Incomplete Surface Accommodation on Non-Equilibrium Heat Transfer in Cavity Flow: A Parallel DSMC Study, *Computers and Fluids*, 45 (2011), 1, pp. 197-201
- [27] Naris, S., Valougeorgis, D., The Driven Cavity Flow over the Whole Range of the Knudsen Number, *Physics of Fluids*, 17 (2005), 9, 097106
- [28] Aoki, K., et al., A Rarefied Gas-Flow Caused by a Discontinuous Wall Temperature, *Physics of Fluids*, 13 (2001), 9, pp. 2645-2661
- [29] Huang, J.-C., et al., A Unified Gas-Kinetic Scheme for Continuum and Rarefied Flows II: Multi-Dimensional Cases, *Communications in Computational Physics*, 12 (2012), 3, pp. 662-690
- [30] Venugopal, V., Girimaji, S. S., Unified Gas Kinetic Scheme and Direct Simulation Monte Carlo Computations of High-Speed Lid-Driven Microcavity Flows, *Communications in Computational Physics*, 17 (2015), 5, pp. 1127-1150
- [31] Wu, L., et al., Oscillatory Rarefied Gas-Flow Inside Rectangular Cavities, *Journal of Fluid Mechanics*, 748 (2014), June, pp. 350-367
- [32] Wang, P., et al., Heat and Mass Transfer of Oscillatory Lid-Driven Cavity Flow in the Continuum, Transition and Free Molecular Flow Regimes, *International Journal of Heat and Mass Transfer*, 13 (2019), 1, pp. 291-300
- [33] Cercignani, C., *The Boltzmann Equation and Its Applications*, Springer-Verlag, New York, USA, 1988
- [34] Milanovic, S., et al., Two-Phase Flow in Channels with Non-Circular Cross-Section of Pneumatic Transport of Powder Material, *Thermal Science*, 22 (2018), Suppl. 5, pp. S1407-S1424
- [35] Hssikou, M., et al., Extended Macroscopic Study of Dilute Gas-flow within a Microcavity, *Modelling and Simulation in Engineering*, 2016 (2016), ID7619746